ACTIVE WIRELESS SENSING IN MULTIPATH ENVIRONMENTS

Thiagarajan Sivanadyan and Akbar Sayeed

Department of Electrical and Computer Engineering
University of Wisconsin - Madison
thiagars@cae.wisc.edu, akbar@engr.wisc.edu

ABSTRACT

Active Wireless Sensing (AWS) was recently proposed as a promising framework for information extraction in wireless sensor networks. In AWS, a wireless information retriever (WIR), equipped with an antenna array, interrogates a select ensemble of sensors with wideband space-time waveforms for rapid and energy-efficient retrieval of sensor information. The WIR extracts sensor information by exploiting the differences in the space-time signatures associated with distinct sensors. In this paper, we investigate the challenging problem of AWS in multipath environments. Our results show that the use of wideband waveforms in AWS allows for exploitation of multipath scattering in two important aspects: higher energy capture and improved sensor resolution, and consequently improved energy efficiency and larger information retrieval rates. These advantages are first quantified through improved reliability and increased capacity of information retrieval for a given sensor transmission energy. A time-reversal technique is also proposed for simultaneously addressing individual sensors. Our results indicate that the richer the multipath, the sharper the ability to address individual sensors while limiting the interference to other sensors. The theoretical development is supported with realistic numerical results.

1. INTRODUCTION

We recently introduced Active Wireless Sensing (AWS) [1, 2] as an alternative and complementary approach to in-network processing for rapid and energy-efficient information retrieval in sensor networks. A key motivation for AWS is to reduce the excess delay and energy consumption associated with in-network processing due to the attendant tasks of information routing and coordination between nodes (see eg. [3]). Technological advances in wideband RF front-ends provide another motivation for AWS. AWS uses a novel distributed architecture shown in Fig. 1(a), in which a Wireless Information Retriever (WIR) queries a select ensemble of nodes to obtain desired information in a rapid and energy-efficient manner. AWS is built on two primary assumptions: i) the sensor nodes are "dumb" in that they have limited computational ability but have relatively sophisticated RF front-ends, and ii) the WIR is computationally powerful, is equipped with an antenna array, and directly interrogates the sensor ensemble with wideband space-time waveforms.

At a conceptual level, AWS is inspired by an intimate connection with communication over multipath channels: the sensors act as active scatterers and produce a multipath response to the WIR's interrogation signals. A key idea behind AWS is to separate multiple sensor responses by resolving the multipath signals in angle and delay and this is facilitated by a virtual representation of wideband space-time wireless channels [4, 5]. In effect, different sensors are associated with distinct angle-delay signatures that can be exploited for simultaneous retrieval of information from the sensor ensemble.

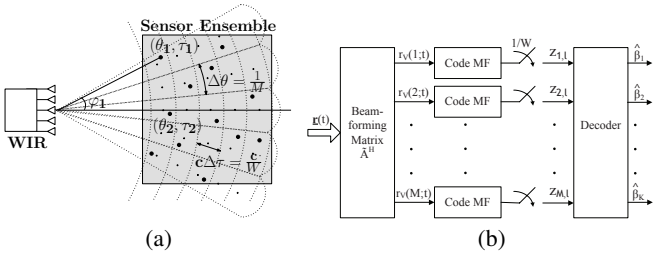

Fig. 1. Active Wireless Sensing. (a) basic communication architecture. (b) Computation of sufficient statistics at the WIR.

While the focus of the initial AWS development was on line-of-sight (LOS) communication [1, 2], in practice, the communication channel is likely to be a multipath channel due to the presence of scattering objects between the sensor ensemble and the WIR. In this paper we address the challenging problem of AWS in the presence of multipath scattering and analyze its impact on performance. Multipath has a detrimental effect on narrowband systems due to the phenomenon of fading. Our results show that the use of wideband waveforms in AWS allows for exploitation of multipath scattering in two important aspects. First, the presence of non-line-of-sight (NLOS) signal paths, in addition to LOS paths, results in a higher capture of sensor signal energy at the WIR, thereby increasing energy efficiency. Second, the presence of multipath scattering increases the degrees of freedom in sensor angle-delay signatures, effectively increasing the sensor resolution at the WIR. Thus, AWS over multipath can accommodate finer-scale sensing and larger information rates compared to LOS environments. We first quantify the above two advantages of scattering both from a reliability and sensing capacity viewpoint. We also propose a simple time-reversal (TR) signaling at the WIR for simultaneously addressing individual sensors. TR signaling is particularly suited to the "dumb sensor" assumption in AWS - it obviates the need for channel estimation at the sensors. Our results indicate that the richer the multipath, the sharper the ability of the WIR to address individual sensors while minimizing interference to other sensors. These results support the well-known "spatial focussing" property of TR methods [6] and indicate the promise of TR methods in the context of AWS.

The next section introduces the basic system model in AWS, the multipath scattering channel and the computation of sufficient statistics at the WIR (see Fig. 1(b)). Section 3 discusses the impact of multipath scattering in increasing signal energy capture and sensor resolution. The impact of these effects on sensing capacity is quantified in Section 4. Section 5 proposes a time-reversal signaling scheme for addressing individual sensors and investigates the impact of scattering on its performance. In all sections, numerical results are provided to support the analysis.

2. SYSTEM MODEL

Consider an ensemble of K sensors randomly distributed over a region of interest, as illustrated in Fig. 1(a). The WIR equipped with an M-element uniform linear array (ULA), initiates information retrieval by sending a signal for training and frequency synchronization. The i-th sensor encodes its measurement in a symbol β_i, modulates a wideband signaling waveform $s_i(t)$ (known at the WIR), of duration T and bandwidth W, by β_i and transmits it with energy $\mathcal{E}$ after a fixed delay (same for all sensors). While different temporal waveforms can be transmitted from different sensors, we focus on the special case in which the same unit-energy spread-spectrum signal, $q(t)$ is transmitted from all sensors. Hence, the transmitted waveform at the i-th sensor is $x_i(t) = \sqrt{\mathcal{E}}\beta_i q(t)$. The transmitted sensor signals pass through a multipath scattering channel consisting of N_p scattering paths (see Fig. 2). The received vector signal at the WIR, $\boldsymbol{r}(t) = [r_1(t), r_2(t), \ldots, r_M(t)]^T$, is a superposition of all the sensor transmissions

$$\boldsymbol{r}(t) = \sqrt{\mathcal{E}} \sum_{i=1}^{K} \beta_i \sum_{n=1}^{N_p} \alpha_{i,n} q(t - \tau_{i,n}) \boldsymbol{a}(\theta_{i,n}) + \boldsymbol{w}(t) \quad (1)$$

where $\tau_{i,n}$ is the relative delay, $\theta_{i,n}$ the angle of arrival (AoA) at the WIR, $\alpha_{i,n}$ the complex path gain of the i-th sensor's signal through the n-th scattering path and $\boldsymbol{w}(t)$ denotes a vector AWGN process with independent components. The ULA unit-norm steering/response vector is denoted by $\boldsymbol{a}(\theta)$ where θ is the normalized angle.[1] Without loss of generality (WLOG), assume that $\min_{i,n} \tau_{i,n} = 0$ and the channel delay spread, $\tau_{max} = \max_{i,n} \tau_{i,n} \ll T$.

2.1. Multipath Scattering Channel

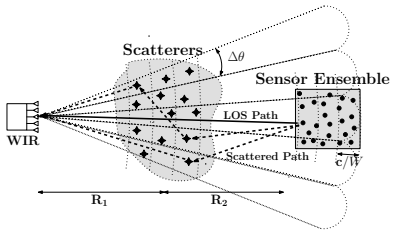

Fig. 2. AWS over a multipath scattering channel.

In (1), the vector channel from the i-th sensor to the WIR is given by

$$\boldsymbol{h}_i(t) = \sum_{n=1}^{N_p} \alpha_{i,n} \delta(t - \tau_{i,n}) \boldsymbol{a}(\theta_{i,n}) \ , \ \boldsymbol{r}(t) = \sum_{i=1}^{K} \boldsymbol{h}_i(t) \star x_i(t) \quad (2)$$

which includes both the LOS component and the scattered (NLOS) components. WLOG, assume that for each sensor, the $n = 1$ path represents the LOS component and the remaining $N_p - 1$ paths are NLOS, as shown in Fig. 2. The complex gains of the scattered paths, $\alpha_{i,n}$, $n = 2, \ldots, N_p$, are generally smaller than that of the LOS components, $\alpha_{i,1}$, since they incur additional losses due to reflections and larger propagation distances. We assume that for each sensor, $|\alpha_{i,1}|^2 = 1$ and $|\alpha_{i,n}|^2 = \sigma_s^2 < 1, n = 2, \ldots, N_p$. We also assume that $\{\theta_{i,n}, \tau_{i,n}\}$ are fixed. The only source of randomness in the channel are the random and independent phases of the path gains $\{\alpha_{i,n}\}$.

[1] θ is related to the physical angle φ as $\theta = d \sin(\varphi)/\lambda$, where d denotes spacing between the antennas and λ the wavelength (see Fig. 1(a)).

2.2. Angle Delay Matched Filtering

We now describe the basic processing of the received signal at the WIR for information retrieval, as illustrated in Fig. 1(b). The received signal $\boldsymbol{r}(t)$ is first projected in M fixed spatial directions and then correlated with uniformly delayed versions of $q(t)$ to yield the sufficient statistics for information retrieval

$$z_{m,\ell} = \int_0^{T+\tau_{max}} \boldsymbol{a}^H(m/M) \boldsymbol{r}(t) q^*(t - \ell/W) dt \quad (3)$$

where $m = -\tilde{M}, \ldots, \tilde{M}$, $\ell = 0, \ldots, L-1$, $\tilde{M} = (M-1)/2$ and $L = \lceil \tau_{max} W \rceil$. The $N_s = M \times L$ angle-delay matched filtered outputs are related to the physical channel in (1) as [1,2]

$$z_{m,\ell} = \sqrt{M\mathcal{E}} \sum_{i=1}^{K} \beta_i \sum_{n=1}^{N_p} \alpha_{i,n} g_{i,n}(m,\ell) + w_{m,\ell} \quad (4)$$

$$\text{where} \ \ g_{i,n}(m,\ell) = \frac{\sin(\pi M(\theta_{i,n} - m/M))}{M \sin(\pi(\theta_{i,n} - m/M))} \text{sinc}(W\tau_{i,n} - \ell).$$

The $N_s \times 1$ vector $\boldsymbol{g}_{i,n} = \{g_{i,n}(m,\ell)\}$ represents the angle-delay signature of the i-th sensor's transmission coupled through the n-th path and satisfies $\|\boldsymbol{g}_{i,n}\|^2 \approx 1$. Let $\boldsymbol{G}_i = [\boldsymbol{g}_{i,1} \cdots \boldsymbol{g}_{i,N_p}]$ and $\boldsymbol{\alpha}_i = [\alpha_{i,1}, \ldots, \alpha_{i,N_p}]^T$. Stacking the MF outputs in a N_s dimensional vector we have

$$\boldsymbol{z} = \sqrt{M\mathcal{E}} \boldsymbol{\Gamma} \boldsymbol{\beta} + \boldsymbol{w} = \sqrt{M\mathcal{E}} \sum_{i=1}^{K} \beta_i \boldsymbol{\gamma}_i + \boldsymbol{w} \quad (5)$$

$$\boldsymbol{\Gamma} = [\boldsymbol{\gamma}_1, \cdots, \boldsymbol{\gamma}_K] = [\boldsymbol{G}_1 \boldsymbol{\alpha}_1, \cdots, \boldsymbol{G}_K \boldsymbol{\alpha}_K] \quad (6)$$

where $\boldsymbol{\Gamma}$ is the $N_s \times K (N_s > K)$ coupling matrix that maps the sensor data vector, $\boldsymbol{\beta} = [\beta_1, \ldots, \beta_K]^T$, to the angle-delay MF output vector $\boldsymbol{z}$ and $\boldsymbol{w}$ is a complex AWGN vector with i.i.d. components of variance σ^2. The vector $\boldsymbol{\gamma}_i = \sum_{n=1}^{N_p} \boldsymbol{g}_{i,n} \alpha_{i,n}$ represents the *angle-delay signature* generated by the i-th sensor at the WIR. The contribution of the scattering paths to the sensors' angle-delay signatures is captured by the virtual path partitioning commensurate with resolution in angle and delay afforded by the signal space [1,4]

$$\gamma_i(m,\ell) \approx \sum_{n \in S_{m,\ell}(i)} \alpha_{i,n} \quad (7)$$

where $S_{m,\ell}(i) = \{n : |\theta_{i,n} - m/M| < 1/2M \ , \ |\tau_{i,n} - \ell/W| < 1/2W\}$ is the set of all paths associated with the i-th sensor whose angles and delays lie within the angle-delay resolution bin of size $\Delta\theta \times \Delta\tau = (1/M) \times (1/W)$ associated with the (m,ℓ)-th angle-delay MF output in (3). It follows from (7) that for a LOS channel, $\boldsymbol{\gamma}_i$ has one dominant non-vanishing component, whereas in multipath environment with spatially distributed NLOS paths, $\boldsymbol{\gamma}_i$ exhibits a larger number of dominant non-vanishing components that are statistically independent since disjoint sets of paths (with independent phases) contribute to distinct components.

2.3. Interference Suppression

Due to the interference between angle-delay signatures of different sensors in (5), we employ a simple linear MMSE interference suppression receiver [7] that exploits the differences in the angle-delay signatures, $\{\boldsymbol{\gamma}_i\}$. Consider independent BPSK sensor transmissions: $\beta_i \in \{-1, 1\}$. The decision at the WIR takes the form $\hat{\boldsymbol{\beta}} = \text{sign}\{\text{Re}(\boldsymbol{L}_{mmse} \boldsymbol{z})\}$ where the $K \times N_s$ filter matrix $\boldsymbol{L}_{mmse} = \boldsymbol{\Gamma}^H \boldsymbol{R}^{-1}$. The correlation matrix, $\boldsymbol{R} = E[\boldsymbol{z}\boldsymbol{z}^H] = M\mathcal{E}\boldsymbol{\Gamma}\boldsymbol{\Gamma}^H + \sigma^2 \boldsymbol{I}$, is used for suppressing interference in the MF outputs, and the matrix $\boldsymbol{\Gamma}^H$ performs angle-delay signature matched filtering. Using a

Gaussian approximation for the interference [7], the instantaneous (conditioned on $\mathbf{\Gamma}$) probability of error for the i-th bit stream an be expressed in terms of the signal to interference and noise ratio (SINR) as $P_e(i) = Q(\sqrt{2\text{SINR}(i)})$, where

$$\text{SINR}(i) = \frac{M\mathcal{E}|{\boldsymbol{\gamma}_i}^H \boldsymbol{R}^{-1}\boldsymbol{\gamma}_i|^2}{\sigma^2\|{\boldsymbol{\gamma}_i}^H\boldsymbol{R}^{-1}\|^2 + M\mathcal{E}\sum\limits_{k\neq i}|{\boldsymbol{\gamma}_i}^H\boldsymbol{R}^{-1}\boldsymbol{\gamma}_k|^2} \quad (8)$$

The long-term P_e is given by $E[Q(\sqrt{2\text{SINR}(i)})]$ where the expectation is over the random path phases in $\mathbf{\Gamma}$. We assume perfect knowledge of $\mathbf{\Gamma}$ at the WIR. In practice, $\mathbf{\Gamma}$ can be estimated at the WIR in a variety of ways [1].

3. IMPACT OF MULTIPATH

This section discusses the impact of multipath scattering on the performance of AWS. From the system equation (6), we note that AWS is equivalent to a Multiple Input Multiple Output (MIMO) system with $\mathbf{\Gamma}$ representing the channel matrix linking the K distributed sensor inputs to the N_s outputs at the WIR. Hence the characteristics of $\mathbf{\Gamma}$ govern the overall performance. In particular, two key channel parameters capture the impact of multipath: the total energy/power contributed by the channel, $\sigma_c^2 = \text{trace}(\mathbf{\Gamma}\mathbf{\Gamma}^H)$, and $\text{rank}(\mathbf{\Gamma})$ that reflects the number of parallel channels (multiplexing gain) created between the sensor ensemble and the WIR.

3.1. Increased Energy Capture

In the absence of scattering, the WIR captures the energy in only the LOS path $\boldsymbol{a}(\theta_{i,1})$ from the i-th sensor. However, scattering paths couple the signal energy from other directions $\boldsymbol{a}(\theta_{i,n})$ to the WIR thereby increasing the fraction of the transmitted sensor energy that is captured by the WIR. To gain insight into the impact of energy capture, we look at the average received SNR of the i-th bit stream

$$E[\text{SNR}(i)] = \frac{M\mathcal{E}E\left[\|\boldsymbol{\gamma}_i\|^2\right]}{\sigma^2} = \frac{M\mathcal{E}(1+(N_p-1)\sigma_s^2)}{\sigma^2} \quad (9)$$

which follows from the assumptions in Sec. 2.1 and since $\|\boldsymbol{g}_{i,n}\|^2 \approx 1$. Thus, the average received SNR increases linearly with the number of paths N_p. The impact of increased energy capture on the probability of error is illustrated in Fig. 3(a) which plots the long-term P_e (see Sec. 2.3) as a function of the per-sensor transmit SNR, $\mathcal{E}/\sigma^2$, averaged across all sensors and over multiple channel (path phases) realizations. The results are for $M = 9$ antennas at the WIR, $K = 108$ sensors and using a spreading code of dimension $N = TW = 127$ for $q(t)$. The scatterers are located half-way between the sensor ensemble and the WIR, as illustrated in Fig. 2. The distances shown are $R_1 + R_2 \approx 2R = 100c/W$, where c is the speed of wave propagation. The scattering paths are spatially distributed so that they occupy distinct angle-delay bins and $\sigma_s^2 = 1/8$.

3.2. Higher Sensor Resolution

In a LOS channel, the ability to distinguish individual sensors is restricted by the physical distance between the sensors relative to the angular and delay resolutions. Therefore in cases where multiple sensors fall within a single angle-delay resolution bin, as shown in Fig. 2, spatially distributed scattering paths are essential for making angle-delay signatures of sensors distinct, as discussed in Sec. 2.2. The $N_s \times K$ ($N_s > K$) channel matrix $\mathbf{\Gamma}$ given in (5) can be separated into the LOS and NLOS components as

$$\begin{aligned} \mathbf{\Gamma} &= [\boldsymbol{\gamma}_1 \cdots \boldsymbol{\gamma}_K] = \mathbf{\Gamma}_{los} + \mathbf{\Gamma}_{mp} \quad (10)\\ \mathbf{\Gamma}_{los} &= [\boldsymbol{\gamma}_{los,1} \cdots \boldsymbol{\gamma}_{los,K}] = [\alpha_{1,1}\boldsymbol{g}_{1,1} \cdots \alpha_{K,1}\boldsymbol{g}_{K,1}]\\ \mathbf{\Gamma}_{mp} &= [\boldsymbol{\gamma}_{mp,1} \cdots \boldsymbol{\gamma}_{mp,K}] = [\mathbf{\Gamma}_{sc,1}\boldsymbol{u}_1 \cdots \mathbf{\Gamma}_{sc,K}\boldsymbol{u}_K] \end{aligned}$$

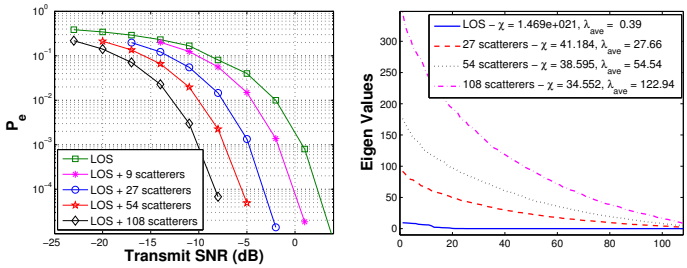

(a) (b)

Fig. 3. (a) P_e vs SNR for different number of scattering paths. $K = 108$, $M = 9$, $N = TW = 127$. (b) Eigenvalues of $\mathbf{\Gamma}\mathbf{\Gamma}^H$.

where the $N_s \times (N_p - 1)$ matrix $\mathbf{\Gamma}_{sc,i}$ represents the signatures associated with the NLOS paths from the i-th sensor and the corresponding gains are $\boldsymbol{u}_i = [\alpha_{i,2}, \ldots, \alpha_{i,N_p}]^T$. When the sensors are spaced sufficiently far apart, $\mathbf{\Gamma}_{los}$ in (10) is full-rank as shown in Fig. 4(a). However, when multiple sensors are closely spaced so that they map to the same angle-delay bin, their LOS signatures are very similar and hence $\mathbf{\Gamma}_{los}$ is rank-deficient. Fig. 4(b) shows $\mathbf{\Gamma}_{los}$ when 108 sensors occupy only 12 distinct angle-delays bins. Simultaneous information retrieval from all sensors is not possible in this case. Multipath scattering is critical in such cases, as discussed next.

When the sensors are closely spaced (say in one angle-delay bin), the angles and delays of the scattering paths from different sensors are also nearly identical, that is, $(\theta_{i,n}, \tau_{i,n}) \approx (\theta_n, \tau_n)$ for $i = 1, \ldots, K$ and $n = 1, \ldots, N_p$. Let $\mathbf{\Gamma}_{sc,i} \approx \mathbf{\Gamma}_{sc} = [\boldsymbol{g}_2, \cdots, \boldsymbol{g}_{N_p}]$ denote the signature matrix of the scatterers and $\boldsymbol{U} = [\boldsymbol{u}_1, \cdots, \boldsymbol{u}_K]$ denote the corresponding $(N_p - 1 \times K)$ complex path gain matrix. From (10), we have

$$\mathbf{\Gamma} = \mathbf{\Gamma}_{los} + \mathbf{\Gamma}_{sc}\boldsymbol{U}\ . \quad (11)$$

If the scatterers are sufficiently far apart, their corresponding angle-delay signatures are linearly independent (nearly orthogonal) and $\mathbf{\Gamma}_{sc}$ is a full rank matrix. Since the entries of $\boldsymbol{U}$ are i.i.d., $\mathbf{\Gamma}$ is full rank with high probability when $N_p > K$. Fig. 4(c) illustrates a full-rank $\mathbf{\Gamma}$ in which the closely spaced sensors corresponding to the rank-deficient $\mathbf{\Gamma}_{los}$ in Fig. 4(b) are coupled to the WIR through an additional 108 spatially distributed NLOS paths. Note the larger number of non-vanishing entries in each signature vector in Fig. 4(c), relative to Fig. 4(a)-(b), as expected from (7). Fig. 3(b) shows the eigenvalue spread of $\mathbf{\Gamma}\mathbf{\Gamma}^H$ for this high sensor density scenario as a function of N_p. The condition number χ of $\mathbf{\Gamma}$ improves with N_p. The increase in the average eigenvalue, λ_{avg}, also reflects the increase in the energy coupled to the WIR as discussed in Sec. 3.1.

4. SENSING CAPACITY

In this section, we further investigate the impact of scattering by quantifying the gains in sensing capacity [2] – the highest rate of information retrieval that may be achieved through coded sensor transmissions. As mentioned earlier, AWS effectively creates a semi-distributed MIMO channel between the K sensors and the N_s MF outputs at the WIR. The capacity of the AWS system is governed by the $N_s \times K$ matrix $\mathbf{\Gamma}$. Using results on the capacity of MIMO channels [8], the sensing capacity of AWS, for a given $\mathbf{\Gamma}$, is given by

$$C(\mathbf{\Gamma}) = \frac{1}{TW+L}\log_2\left|\boldsymbol{I} + \frac{\mathcal{E}M}{\sigma^2}\mathbf{\Gamma}\mathbf{\Gamma}^H\right| \text{ b/s/Hz} \quad (12)$$

which reflects the mutual information between the K sensor inputs and N_s MF outputs, under the assumption of equal power and independent Gaussian signaling from the sensors, and $TW + L =$

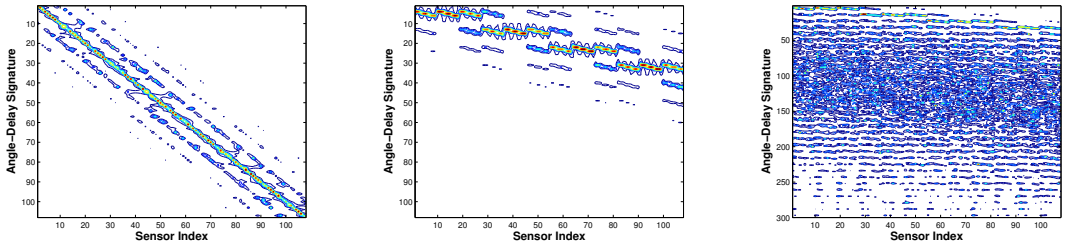

(a) (b) (c)

Fig. 4. (a) $\mathbf{\Gamma}_{los}$ when 108 sensors occupy distinct angle-delay bins. (b) & (c) $\mathbf{\Gamma}_{los}$ and $\mathbf{\Gamma}$, respectively, when 108 sensors occupy only 12 distinct angle-delay bins and $\mathbf{\Gamma}$ corresponds to $N_p = 108$ spatially distributed paths.

$(T + \tau_{max})W$ is the signaling time-bandwidth product for each channel use. The sensing capacity can also be expressed in terms of the eigenvalues, $\{\lambda_i\}$, of $\mathbf{\Gamma}\mathbf{\Gamma}^H$

$$C(\mathbf{\Gamma}) = \frac{1}{TW + L} \sum_{i=1}^{K_{eff}} \log_2 \left(1 + \frac{\mathcal{E}M}{\sigma^2}\lambda_i\right) \tag{13}$$

where $1 \leq K_{eff} \leq K$ reflects the rank of the matrix $\mathbf{\Gamma}\mathbf{\Gamma}^H$ and represents the number of parallel channels created between the sensor ensemble and the WIR. The long-term capacity is given by $C = E[C(\mathbf{\Gamma})]$, where the expectation is over the statistics of the independent phases of path gains $\{\alpha_{i,n}\}$ (see (6)) in (12) and over the statistics of the eigenvalues in (13).

The effect of increased energy capture on sensing capacity is illustrated in Fig. 5(a), which plots $E[C(\mathbf{\Gamma})]$ as a function of per-sensor transmit SNR, $\mathcal{E}/\sigma^2$, for different values of N_p. In this simulation, $K = 108$ sensors are placed sufficiently far apart (occupy distinct angle-delay bins) and hence $\mathbf{\Gamma}$ is always full rank, as discussed in Sec. 3.2, and $K_{eff} = K$. The upward shift in the capacity curves with increasing N_p is due to the increase in size of the eigenvalues λ_i with N_p, reflecting the increased energy coupled through the multipath channel.[2] Fig. 5(b) shows the impact of scattering on sensing capacity when the 108 sensors are closely spaced (their LOS paths occupy only 6 distinct angle-delay bins) so that $\mathbf{\Gamma}_{los}$ is rank-deficient (see Sec. 3.2). In this case, the increase in the sensing capacity with N_p is due to two effects. First, the spatially distributed NLOS paths increase $K_{eff} = \text{rank}\left(\mathbf{\Gamma}\mathbf{\Gamma}^H\right)$ which is reflected in the increasing slope of the capacity plots as N_p increases. Second, the curves for larger N_p are higher due to the higher energy capture as in the previous case.

5. TIME REVERSED SIGNALING TO ADDRESS INDIVIDUAL SENSORS

In this section, we investigate the impact of multipath scattering on downlink communication in AWS. One of the attractive features of AWS is the ability of the WIR to "program" the sensors for different tasks. This requires that the WIR be able to individually address different sensors. We propose a simple time-reversed (TR) signaling scheme - based on the sensors' signature vectors - which may be exploited by the WIR for simultaneously addressing individual sensors. TR signaling has the well-known property of "spatial focusing" in a desired direction in rich scattering environments [6]. Our initial results indicate that TR signaling is a promising mechanism for the WIR to individually address sensors in a multipath scattering environment, *without* knowing their locations, and without the need for channel estimation at the sensors. Furthermore, the richer the multipath, the sharper the ability to focus the signal at the desired sensor while minimizing the interference to other sensors.

[2] $E[\sigma_c^2] = E[\text{trace}(\mathbf{\Gamma}\mathbf{\Gamma}^H)] = \sum_{i=1}^{K_{eff}} E[\lambda_i] = K_{eff}(1+(N_p-1)\sigma_s^2)$.

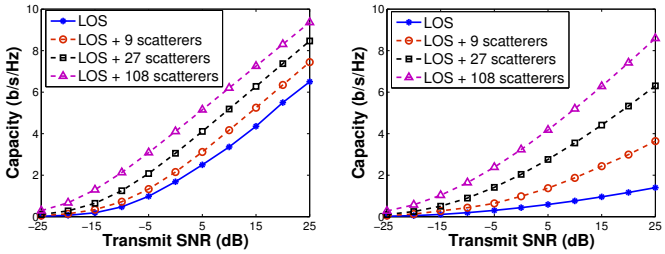

(a) (b)

Fig. 5. Sensing capacity of AWS as a function of the transmit SNR for different values of N_p. (a) 108 sensors occupy distinct angle-delay bins. (b) 108 sensors occupy 6 distinct angle-delay bins.

The TR space-time signal transmitted from the WIR to address the i-th sensor is given by

$$\boldsymbol{s}_{tr,i}(t) = \sqrt{\frac{\mathcal{E}}{c_1}} \sum_{\ell=0}^{L-1} \sum_{m=-\tilde{M}}^{m=\tilde{M}} \gamma_i^*(m,\ell)\boldsymbol{a}^*\left(\frac{m}{M}\right) q^*\left(\tilde{T} - t - \frac{\ell}{W}\right) \tag{14}$$

where $0 \leq t \leq \tilde{T}$, $\tilde{T} = T + \tau_{max}$, $c_1 = E[\|\boldsymbol{\gamma}_i\|^2] \approx 1 + (N_p - 1)\sigma_s^2$, and the normalization ensures that the transmitted signal has average energy $\mathcal{E}$. The received TR signal at the k-th sensor is

$$r_{tr,k}(t) = \sum_{n=1}^{N_p} \alpha_{k,n}\boldsymbol{a}^T(\theta_{k,n}) s_{tr,i}(t - \tau_{k,n}) + w(t) \tag{15}$$

$$\overset{(a)}{=} \sqrt{\frac{\mathcal{E}}{c_1}} \sum_{\ell,m,n_1,n_2} \alpha_{k,n_1}\alpha_{i,n_2}^* g_{i,n_2}^*(m,\ell)\boldsymbol{a}^T(\theta_{k,n_1}) \boldsymbol{a}^*\left(\frac{m}{M}\right) q^*\left(\tilde{T} - t + \tau_{k,n_1} - \frac{\ell}{W}\right) + w(t) \tag{16}$$

where $w(t)$ denotes an AWGN process and (a) is obtained using (14) and substituting $\gamma_i(m,\ell) = \sum_{n=1}^{N_p} \alpha_{i,n} g_{i,n}(m,\ell)$ from (6). The received signal $r_{tr,k}(t)$ is matched filtered at the k-th sensor with $q(t)$ and the corresponding MF output at time τ is

$$z_{tr,k}(\tau) = \int r_{tr,k}(t) q(\tau - t) dt \tag{17}$$

$$= \sqrt{\frac{\mathcal{E}}{c_1}} \sum_{\ell,m,n_1,n_2} \alpha_{k,n_1}\alpha_{i,n_2}^* g_{i,n_2}^*(m,\ell)\boldsymbol{a}^T(\theta_{k,n_1})\boldsymbol{a}^*\left(\frac{m}{M}\right) \int q^*\left(\tilde{T} - t + \tau_{k,n_1} - \frac{\ell}{W}\right) q(\tau - t) dt + w(\tau) \tag{18}$$

where $w(\tau)$ is a complex Gaussian noise variable with variance σ^2. The received SNR at the target (i-th) sensor is maximized at $\tau = \tilde{T}$

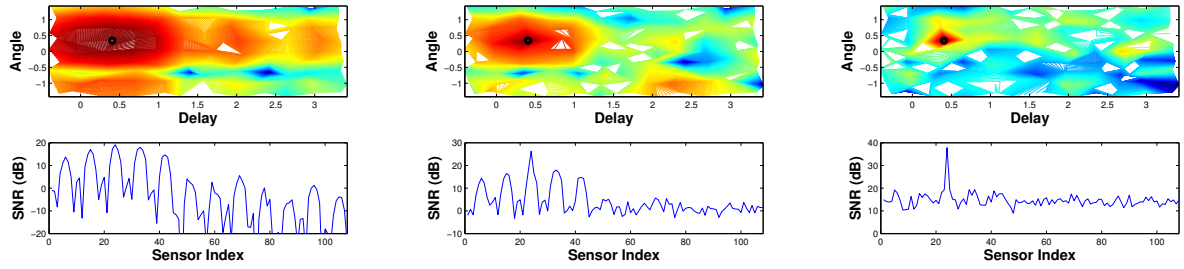

(a) (b) (c)

Fig. 6. The strength of the received TR signal at different sensor for different values of N_p; a black circle indicates the target sensor (sensor 24) in the contour plots; 108 sensors occupy 12 distinct angle-delay bins. (a) LOS paths only. (b) LOS + 9 NLOS scattering paths. (c) LOS + 54 NLOS scattering paths.

and the MF output at the k-th sensor at this 'optimum' time is

$$\begin{aligned} z_{tr,k}(\tilde{T}) &\approx \sqrt{\frac{\mathcal{E}}{c_1}} \sum_{\ell,m,n_1,n_2} \alpha_{k,n_1}\alpha^*_{i,n_2} g^*_{i,n_2}(m,\ell)\boldsymbol{a}^T(\theta_{k,n_1}) \\ &\quad \boldsymbol{a}^*\left(\frac{m}{M}\right)\mathrm{sinc}(W\tau_{k,n_1}-\ell)+w(\tilde{T}) \\ &= \sqrt{\frac{\mathcal{E}}{c_1}} \sum_{\ell,m,n_1,n_2} \alpha_{k,n_1}\alpha^*_{i,n_2} g^*_{i,n_2}(m,\ell) g_{k,n_1}(m,\ell)+w(\tilde{T}) \\ &= \sqrt{\frac{\mathcal{E}}{c_1}} {\boldsymbol{\gamma_i}}^H \boldsymbol{\gamma_k} + w(\tilde{T})\,. \end{aligned} \tag{19}$$

Thus, at the optimal sampling time, the SNR at the k-th sensor is $\frac{\mathcal{E}|{\boldsymbol{\gamma_i}}^H\boldsymbol{\gamma}_k|^2}{\sigma^2 E[\|\boldsymbol{\gamma}_i\|^2]}$ which is maximum at the target sensor ($k=i$). Fig. 6 plots the value of the SNR at different sensors for different values of N_p. The contour plots correspond to magnitude of the MF output $|z_{tr,k}(\tilde{T})|^2$. Note that with increasing N_p, the SNR of the received TR signal increases at the target sensor, whereas it decreases at the other sensors. This is because of the increasing number of non-vanishing statistically independent components in the signature vectors with increasing N_p (see Secs. 2.2 and 3.2).

We can further quantify the impact of scattering on the performance of TR signaling by considering the ratio of the average signal power to the average interference and noise power (a modified SINR) when two sensors (i and k) are simultaneously addressed

$$\widehat{\mathrm{SINR}}(i) = \frac{\mathcal{E}E[\|\boldsymbol{\gamma}_i\|^4]/c_1}{\sigma^2+\mathcal{E}E[|{\boldsymbol{\gamma_i}}^H\boldsymbol{\gamma_k}|^2]/c_1}. \tag{20}$$

Using (6) and (19), we can approximate the signal power and the interference power in the limit of large N_p as

$$E[\|\boldsymbol{\gamma}_i\|^4] \approx N_p^2\sigma_s^4\hat{E}_n\left[|\boldsymbol{g}^H_{i,n}\boldsymbol{g}_{i,n}|^2+|\boldsymbol{g}^H_{i,n}\boldsymbol{g}_{i,n'}|^2\right] \tag{21}$$

$$\approx N_p^2\sigma_s^4\left(1+\hat{E}_n\left[|\boldsymbol{g}^H_{i,n}\boldsymbol{g}_{i,n'}|^2\right]\right) \tag{22}$$

$$E[|{\boldsymbol{\gamma_i}}^H\boldsymbol{\gamma_k}|^2] \approx N_p^2\sigma_s^4\hat{E}_n\left[|\boldsymbol{g}^H_{i,n}\boldsymbol{g}_{k,n'}|^2\right] \tag{23}$$

where $\hat{E}_n$ represents the average over all the scattering paths. In general, the TR signaling is interference limited since the SINR saturates as the transmit SNR ($\mathcal{E}/\sigma^2$) is increased

$$\widehat{\mathrm{SINR}}(i) \to \frac{1+\mathrm{E}\left[|\boldsymbol{g}^H_{i,n}\boldsymbol{g}_{i,n'}|^2\right]}{\mathrm{E}\left[|\boldsymbol{g}^H_{i,n}\boldsymbol{g}_{k,n'}|^2\right]} \text{ as } \frac{\mathcal{E}}{\sigma^2}\to\infty\,. \tag{24}$$

The SINR scaling behavior is illustrated in Fig. 7 which plots $\widehat{\mathrm{SINR}}(i)$ as a function of the transmit SNR, $\mathcal{E}/\sigma^2$, for different values of N_p. When the sensors are sufficiently spaced (distinct angle-delay bins), as in Fig. 7(a), the SINR saturates at the value given by (24), regardless of the number of paths, since the sensors' angle-delay signatures are nearly orthogonal even in the LOS scenario. On the other hand, when the sensors are closely spaced, as in Fig. 7(b), the SINR saturates to the maximum value in Fig. 7(a) only in the case of 54 scattering paths - the SINR saturates to a lower value for fewer paths since they are not sufficient to make the angle-delay signatures sufficiently distinct. This is consistent with the impact of scattering in increasing the rank of $\boldsymbol{\Gamma}$ for closely spaced sensors.

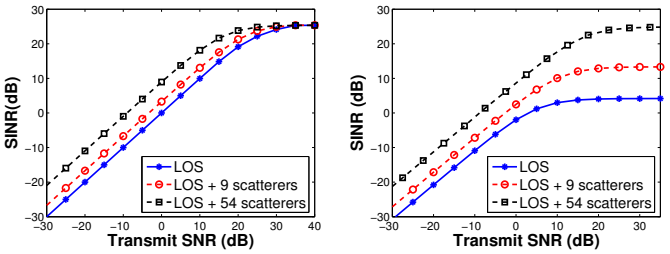

(a) (b)

Fig. 7. $\widehat{\mathrm{SINR}}$ vs transmit SNR $\mathcal{E}/\sigma^2$. (a) 108 sensors occupy distinct angle-delay bins. (b) 108 sensors occupy only 12 distinct angle-delay bins.

6. REFERENCES

[1] T. Sivanadyan and A. Sayeed, "Active Wireless Sensing for Rapid Information Retrieval in Sensor Networks", *Proc. 5th Intl. Conf. on Information Processing in Sensor Networks*, Apr. 2006.

[2] A. Sayeed and T.Sivanadyan, "Source Channel Communication Protocols and Tradeoffs in Active Wireless Sensing", *Proc. 44th Annual Allerton Conference on Communication, Control and Computing*, Sep. 2006.

[3] D. Estrin, L. Girod, G. Pottie and M. Srivastava, "Instrumenting the world with wireless sensor networks", *Proc. IEEE Intl. Conf. on Acoustics, Speech, and Signal Processing*, May 2001.

[4] A. Sayeed, "Deconstructing Multi-antenna Fading Channels", *IEEE Trans. on Signal Processing*, Oct. 2002.

[5] A. Sayeed, "A Virtual Representation for Time- and Frequency-Selective Correlated MIMO Channels", *Proc. IEEE Intl. Conf. on Acoustics, Speech, and Signal Processing*, May 2003.

[6] M. Fink, "Time Reversed Acoustics", *Physics Today*, Mar. 1997.

[7] S. Verdu,"Multiuser Detection", Cambridge University Press, 1998.

[8] E. Telatar,"Capacity of Multi-Antenna Gaussian Channels", *AT&T-Bell Labs Internal Tech. Memo.*, Jun. 1995.